^{6}Li in a three-body model with realistic Forces: Separable versus nonseparable approach

L. Hlophe, Jin Lei, Ch. Elster, A. Nogga, and F. M. Nunes

Phys. Rev. C **96**, 064003 — Published 26 December 2017

DOI: 10.1103/PhysRevC.96.064003

^{6}Li in a Three-Body Model with Realistic Forces: Separable vs. Non-separable Approach

L. Hlophe[(a)], Jin Lei[(b)], Ch. Elster[(b)], A. Nogga[(c)], and F.M. Nunes[(a)]
(a) National Superconducting Cyclotron Laboratory and Department of Physics and Astronomy, Michigan State University, East Lansing, MI 48824, USA
(b)Institute of Nuclear and Particle Physics, and Department of Physics and Astronomy, Ohio University, Athens, OH 45701, USA
(c) IAS-4, IKP-3, JHCP, and JARA-HPC, Forschungszentrum Jülich, D-52428 Jülich, GER
(Dated: November 29, 2017)

Background: Deuteron induced reactions are widely used to probe nuclear structure and astrophysical information. Those (d,p) reactions may be viewed as three-body reactions and described with Faddeev techniques.

Purpose: Faddeev equations in momentum space have a long tradition of utilizing separable interactions in order to arrive at sets of coupled integral equations in one variable. However, it needs to be demonstrated that their solution based on separable interactions agrees exactly with solutions based on non-separable forces.

Methods: Momentum space Faddeev equations are solved with non-separable and separable forces as coupled integral equations.

Results: The ground state of ^{6}Li is calculated via momentum space Faddeev equations using the CD-Bonn neutron-proton force and a Woods-Saxon type neutron(proton)-^{4}He force. For the latter the Pauli-forbidden S-wave bound state is projected out. This result is compared to a calculation in which the interactions in the two-body subsystems are represented by separable interactions derived in the Ernst-Shakin-Thaler framework.

Conclusions: We find that calculations based on the separable representation of the interactions and the original interactions give results that agree to four significant figures for the binding energy, provided that energy and momentum support points of the EST expansion are chosen independently. The momentum distributions computed in both approaches also fully agree with each other.

PACS numbers: 21.45.-v,27.20.+n

I. INTRODUCTION

A variety of applications of nuclear physics require the understanding of neutron capture on unstable nuclei. Due to the short lifetimes involved, direct measurements are currently not possible, and thus indirect methods using (d,p) reactions have been used for both the direct capture [1, 2] as well as the compound [3] components. A recent review on (d,p) reactions and its connection to neutron capture can be found in [4]. In addition, single neutron transfer (d,p) reactions can be used to constrain proton capture cross sections, due to mirror symmetry (e.g. [5]). Beyond these astrophysical motivations, single-nucleon transfer reactions involving the deuteron have been the preferred tool to study shell evolution in nuclear structure, both for nuclei close and far from stability (see Refs. [6, 7] for two recent examples). In all these cases, a reliable reaction theory for (d,p) is a critical ingredient.

Scattering and reaction processes involving deuterons either as projectile or as target are perhaps the most natural three-body problem in the realm of nuclear reactions. The binding energy of the deuteron is so small that its root-mean-square radius is significantly larger than the range of the force. That means that when a deuteron interacts with a compact, well bound nucleus, one may expect that it will behave like a three-body system consisting of proton p, a neutron n, and a nucleus A. The obvious three-body reactions are elastic scattering, rearrangement and breakup processes. In order to describe those processes on the same footing, deuteron-nucleus scattering should be treated at least at the three-body level. Note that if the target itself has low-lying excitations, one may need to go beyond the pure three-body treatment, see e.g. [8]. However, for the application we consider here (namely ^{6}Li $\equiv n+p+\alpha$), one expects the three-body treatment to be sufficient.

The three-body Hamiltonian governing the dynamics of the (d,p) reactions contains the well understood nucleon-nucleon (NN) interaction as well as an effective interaction between the nucleons and the target. Commonly these nucleons-nucleus interactions are parameterized by phenomenological optical potentials which fit a large body of elastic scattering data [9–11].

The application of momentum space Faddeev techniques to nuclear reactions has been pioneered in Ref. [12], and successfully applied to (d,p) reactions for light nuclei [13]. However, when extending these calculations to heavier nuclei [14, 15], it becomes apparent that the screening techniques employed for incorporating the Coulomb interaction in Faddeev-type reaction calculations with light nuclei cannot be readily extended to the heaviest nuclei. Therefore, a new method for treating (d,p) reactions with the exact inclusion of the Coulomb force as well as target excitation was formulated in Ref. [16]. This new approach relies on a separable representation of the pairwise forces.

Separable representations of the forces between constituents forming the subsystems in a Faddeev approach have a long tradition in few-body physics. In the context of describing light nuclei like ^{6}Li [17–19] and ^{6}He [20] in a three-body approach, rank-1 separable interactions of Yukawa-type have been successfully used. In the case of the three-nucleon problem, separable representations for the NN force of higher rank had to be developed in order to improve the agreement with exact Faddeev calculations [21–24]. Those were based on the scheme suggested by Ernst-Shakin-Thaler [25] (EST).

The pioneering work of Hlophe and collaborators [26–28] demonstrated that an EST-based separable interaction of rank up to 5 provides a precise description of nucleon-nucleus elastic scattering for a wide range of energies, including nuclei as heavy as ^{208}Pb. The development of these separable complex (and energy dependent) effective potentials opens the path to apply the method of Ref. [16] to the three-body $A(d,p)B$ reaction problem.

Since a separable expansion of the nuclear transition amplitudes can be viewed as a basis expansion, it is critical to understand the convergence of the numerical results. In order to benchmark these calculations, one needs to compare to the solution of the problem without the use of separable interactions. Such a comparison was successfully carried out for neutron-deuteron scattering at 10 MeV [29], and at slightly higher energies in Ref. [30]. Both studies showed that, for a converged expansion of the force in the two-body subsystems, observables in the three-body system agree.

For the applications we have in mind, the benchmarks need to be performed for the $A+d$ case in a regime for which non-separable solutions are possible and exact. Furthermore, our work aims to establish that the approach based on separable two-body transition matrices is *equivalent* to the approach using those transition matrices directly, given the convergence in the expansion. We choose as benchmark, the ground state of ^{6}Li because there is a large number of reference calculations in the literature; our goal is for an agreement between the separable and the non-separable approach of up to four significant figures in the binding energy. The ultimate goal is to apply the separable approach to nuclear reactions. Here we expect to lose some precision in solving the Faddeev equations in the continuum. Note that benchmarks performed for the four-nucleon bound state ensured 4 digit accuracy [31] while the corresponding work for positive energies provided only a 2-digit accuracy [32]. This should also be sufficient for the problem we are considering, particularly when computing (d,p) observables.

In this work, our EST-based separable expansion uses off-shell transition amplitudes at negative energies as basis states. Those states depend on two parameters, namely the energy and the off-shell asymptotic momentum, which are chosen independently. This is in contrast to previous work on the neutron-deuteron system [21, 22], which did not explore the full parameter space. The effective interactions in the neutron-alpha and proton-alpha channels are given

by a Woods-Saxon type potential fitted to phase shifts in the S- and P-wave channels. Since the $n\alpha$ Woods-Saxon potential supports a bound state in the S-wave two-body channel, which is Pauli forbidden, we derive a projection scheme for both approaches which differs from previous works [18, 33] in that it does not add additional Faddeev components, but rather only modifies the respective two-body transition amplitudes.

In Sec. II a brief summary of the theory is provided, including the three-body equations we solve and the new formulation used to project out the Pauli forbidden S-wave state in the neutron(proton)-alpha channel. The inputs to the problem are presented in Sec. III A, including the interactions that govern the two-body subsystems, and the results for the ^{6}Li binding energy and wavefunction are discussed in Sec. III B and III C. Our findings are summarized in Sec. IV.

II. FORMAL CONSIDERATIONS

A. Faddeev Equations for the ground state of ^{6}Li

The bound state of three particles with masses m_i, m_j, and m_k and spins j_i, j_j, and j_k which interact via pairwise forces $V^i \equiv V_{jk}$ ($i, j, k = 1, 2, 3$ and cyclic permutations thereof) is given by the Schrödinger equation, which reads in integral form

$$|\Psi\rangle = G_0(E_3) \sum_{i=1}^{3} V^i |\Psi\rangle. \tag{1}$$

Here the free propagator is given by $G_0(E) = (E_3 - H_0)^{-1}$, where H_0 stands for the free Hamiltonian and E_3 for the binding energy of the three-body system. Introducing Faddeev components

$$|\Psi\rangle = \sum_{i=1}^{3} |\psi_i\rangle \equiv |\psi_{jk}\rangle + |\psi_{ki}\rangle + |\psi_{ij}\rangle, \tag{2}$$

with

$$|\psi_i\rangle = G_0(E_3) V^i |\Psi\rangle, \tag{3}$$

leads to three coupled integral equations for the three components $|\psi_{i,j,k}\rangle$,

$$|\psi_i\rangle = G_0(E_3)\ t_i \sum_{j \neq i} |\psi_j\rangle. \tag{4}$$

The operator $t_i = V^i + V^i G_0(E_3) t_i$ describes the two-body t-matrix in the subsystem jk. In order to solve Eqs. (4) standard Jacobi momenta are used,

$$\begin{aligned} \vec{p}_k \equiv \vec{p}_{ij} &= \mu_{ij} \left(\frac{\vec{k}_i}{m_i} - \frac{\vec{k}_j}{m_j} \right) \\ \vec{q}_k \equiv \vec{q}_{ij} &= \mu_{3b,k} \left(\frac{\vec{k}_k}{m_k} - \frac{\vec{k}_i + \vec{k}_j}{m_i + m_j} \right). \end{aligned} \tag{5}$$

Here the two-body reduced mass μ_{ij} and the three-body reduced mass $\mu_{3b,k}$ are given by

$$\begin{aligned} \mu_{ij} &= \frac{m_i m_j}{m_i + m_j} \\ \mu_{3b,k} &= \frac{m_k (m_i + m_j)}{M}, \end{aligned} \tag{6}$$

with $M = m_i + m_j + m_k$ being the total mass of the system.

Instead of using a three-dimensional Jacobi basis, we expand into momentum eigenstates which depend on the magnitude of the momenta and angular momentum eigenstates. The orbital angular momenta of the three particles are coupled to total angular momentum J and its third component M_J,

$$|p_k q_k \alpha_k\rangle_{(ij)k} = |p_k q_k ((l_k (j_i j_j) s) J_{ij} (\lambda_k j_k) J_k) J M_J\rangle_{(ij)k}, \tag{7}$$

which are normalized as

$$ {}_{(ij)k}\langle p'_k q'_k \alpha'_k | p_k q_k \alpha_k \rangle_{(ij)k} = \frac{\delta(p'_k - p_k)}{p'_k p_k} \frac{\delta(q'_k - q_k)}{q'_k q_k} \delta_{\alpha'_k \alpha_k}. \tag{8} $$

The notation $(ij)k$ indicates that k is the spectator.

Since we represent each Faddeev component $|\psi_k\rangle$ in its natural set of Jacobi coordinates $|p_k q_k \alpha_k\rangle_{(ij)k}$, a transformation between the sets $(jk)i$ to $(ij)k$ and $(ki)j$ to $(ij)k$ is required. The partial wave representation of these transformations can be calculated as outlined in [34] and can be written as an integral over the cosine x of the relative angle of p_k and q_k of the Faddeev components evaluated at shifted momenta $\pi'_j = \pi'_j(p'_k q_k x)$ and $\chi'_j = \chi'_j(p'_k q_k x)$. All geometrical information can be parameterized by functions $\mathcal{G}_{\alpha'_k \alpha'_j}(p'_k q_k x)$. We give more details on these transformations in Appendix A.

Inserting complete sets of states in Eqs. (4) and making use of the geometrical coefficients $\mathcal{G}_{\alpha'_k \alpha'_j}(p'_k q_k x)$, we arrive at a set of three coupled Faddeev equations:

$$ \begin{aligned} \psi_k^{\alpha_k}(p_k, q_k) = G_0(E_{q_k}; p_k) \sum_{\alpha'_k} \int dp'_k p'^2_k \; t_k^{\alpha_k \alpha'_k}(p_k, p'_k; E_{q_k}) \\ \times \int_{-1}^{1} dx \left[\sum_{\alpha'_i} \mathcal{G}_{\alpha'_k \alpha'_i}(p'_k q_k x) \; \psi_i^{\alpha'_i}(\pi'_i, \chi'_i) + \sum_{\alpha'_j} \mathcal{G}_{\alpha'_k \alpha'_j}(p'_k q_k x) \; \psi_j^{\alpha'_j}(\pi'_j, \chi'_j) \right], \end{aligned} \tag{9} $$

where we introduced the pair kinetic energy $E_{q_k} = E_3 - \frac{q_k^2}{2\mu_{3b,k}}$ and the free three-body propagator

$$ G_0(E_{q_k}; p_k) = \frac{1}{E_{q_k} - \frac{p_k^2}{2\mu_{ij}}} \; . \tag{10} $$

The two-body t-matrix $t_k^{\alpha_k \alpha'_k}$ in the Jacobi coordinates $(ij)k$ is given by the Lippmann-Schwinger equation (LSE),

$$ t_k^{\alpha_k \alpha'_k}(p_k, p'_k; E_{q_k}) = V^{k;\alpha_k \alpha'_k}(p_k, p'_k) + \sum_{\alpha''} \int \mathrm{d}p''_k p''^2_k \; V^{k;\alpha_k \alpha''_k}(p_k, p''_k) \; G_0(E_{q_k}; p''_k) \; t_k^{\alpha''_k \alpha'_k}(p''_k, p'_k; E_{q_k}). \tag{11} $$

For brevity, we labeled the partial wave channels using three-body quantum numbers α_k. Since the LSE corresponds to a two-body problem at an off-shell energy E_{q_k}, the interactions and t matrices will only dependent on quantum numbers of the two-body subsystems and will be diagonal in the spectator quantum numbers.

As is well known (see e.g. [35]), if the t matrix in the subsystems is separable,

$$ t_k^{\alpha_k \alpha'_k}(p_k, p'_k; E_{q_k}) = \sum_{mn} h_m^{\alpha_k}(p_k) \; \tau_{mn}^{\alpha_k \alpha'_k}(E_{q_k}) \; h_n^{\alpha'_k}(p'_k), \tag{12} $$

the coupled integral equations in two variables, Eqs. (9), can be reduced to coupled integral equations in one variable (see Eq. (A5)). The indices $\{m, n\}$ represent the rank of the separable potential, and k stands for the index of the Faddeev component. It is possible, with an appropriate choice of integration variables and the introduction of the modified geometric functions $\tilde{\mathcal{G}}_{\alpha'_k \alpha'_j}(q_i q_k x)$ as defined by Eq. (A6), to obtain a separable form for the Faddeev amplitudes:

$$ \psi_k^{\alpha_k}(p_k, q_k) \equiv G_0(E_{q_k}, p_k) \; \sum_m h_m^{\alpha_k}(p_k) \; F_{m\alpha_k}^{(k)}(q_k). \tag{13} $$

Reinserting the above expressing into Eqs. (9) leads to a coupled set of equations for the amplitudes $F_{m\alpha_k}^{(k)}(q_k)$,

$$ \begin{aligned} F_{m\alpha_k}^{(k)}(q_k) = \sum_{\nu\alpha'_i} \int d\tilde{q}_i \; \tilde{q}_i^2 \left[\sum_{n\alpha'_k} \tau_{mn}^{\alpha_k \alpha'_k}(E_{q_k}) \; Z_{n\alpha'_k, \nu\alpha'_i}^{(ki)}(q_k, \tilde{q}_i) \right] F_{\nu\alpha'_i}^{(i)}(\tilde{q}_i) \\ + \sum_{\nu\alpha'_j} \int d\tilde{q}_j \; \tilde{q}_j^2 \left[\sum_{n\alpha'_k} \tau_{mn}^{\alpha_k \alpha'_k}(E_{q_k}) \; Z_{n\alpha'_k, \nu\alpha'_j}^{(kj)}(q_k, \tilde{q}_j) \right] F_{\nu\alpha'_j}^{(j)}(\tilde{q}_j), \end{aligned} \tag{14} $$

where all amplitudes are generated by cyclic permutations of (ijk). The functions $Z_{n\alpha'_k, \nu\alpha'_k}^{(ki)}(q_k, \tilde{q}_i)$ are the so-called transition amplitudes [35] coupling the different types of subsystems. For completeness, the expressions are explicitly given in Appendix A. We solve both sets of Faddeev equations using iterative Lanczos-type techniques [36].

B. Treatment of Pauli Blocking in the Faddeev Equations

Three-body models of nuclei or nuclear reactions require taking Pauli blocking into account to remove components of the wavefunction that would disappear under full anti-symmetrization of the (A+2)-body problem. Though this topic has already been extensively treated in the literature (see e.g. [18, 33, 37–39]), we need to pick it up again and develop a formulation for projecting out a Pauli forbidden state in momentum space Faddeev equations that works for separable and non-separable forces alike.

Let us assume that the Pauli forbidden state is created by a potential V^i in the subsystem i. This two-body bound state with the wave function $|\phi^i\rangle$ is a normalized eigenstate of $H^i = H_0 + V^i$. It can be projected out by introducing the channel Hamiltonian

$$\tilde{H}^i = H_0 + V^i + \hat{V}^i = H^i + \tilde{V}^i, \tag{15}$$

where $\hat{V}^i = \lambda|\phi^i\rangle\langle\phi^i|$ with λ being a large number. The Faddeev equations require two-body transition matrices as input. Thus one needs

$$\tilde{t}_i(z) = \tilde{V}^i + \tilde{V}^i G_0(z)\tilde{t}_i(z), \tag{16}$$

with $G_0(z)$ being the free resolvent with $z = E + i\varepsilon$. In this derivation we will drop the subscript i, representing the arrangement channel, for brevity. The discussion is general for each pair that contains forbidden states. Using the Gell-Mann-Goldberger relation [40] in the form

$$\tilde{t}(z) = t(z) + \big(1 + VG(z)\big)\,\hat{t}(z)\,\big(1 + G(z)V\big), \tag{17}$$

where $G^{-1}(z) = (z - H)$, and $\hat{t}(z)$ an operator fulfilling the LSE,

$$\hat{t}(z) = \hat{V} + \hat{V}G(z)\hat{t}(z) = \hat{V} + \hat{V}\tilde{G}(z)\hat{V}. \tag{18}$$

Here $\tilde{G}^{-1}(z) = (z - \tilde{H})$. Since $\hat{V}$ is separable and of rank-1, the analytic solution for $\hat{t}$ is separable and of rank-1,

$$\hat{t}(z) = |\phi\rangle\,\frac{1}{\frac{1}{\lambda} - \langle\phi|G(z)|\phi\rangle}\,\langle\phi|. \tag{19}$$

Using $VG(z) = t(z)G_0(z)$ Eq. (17) becomes

$$\tilde{t}(z) = t(z) + \frac{|\eta(z)\rangle\langle\bar{\eta}(z)|}{\frac{1}{\lambda} - \frac{1}{z - E_b}}, \tag{20}$$

where E_b represents the two-body energy for the bound state b that needs to be projected out, and

$$\begin{aligned} |\eta(z)\rangle &= \big(1 + t(z)G_0(z)\big)|\phi\rangle\ , \\ \langle\bar{\eta}(z)| &= \langle\phi|\big(1 + G_0(z)t(z)\big). \end{aligned} \tag{21}$$

Equation (20), already presented in Ref. [41], allows to take the limit $\lambda \to \infty$ analytically. It remains to express the states in Eq. (21) in a more convenient fashion. Inserting the identity $\mathbf{1} = G_0^{-1}(z)G_0(z)$ and using the representation $G(z) = G_0(z) + G_0(z)t(z)G_0(z)$ of the full resolvent leads to

$$\begin{aligned} |\eta(z)\rangle &= (1 + t(z)G_0(z))|\phi\rangle \\ &= (z - H_0)G(z)|\phi\rangle \\ &= (z - H_0)\frac{1}{z - E_b}|\phi\rangle \end{aligned} \tag{22}$$

Similarly, one obtains

$$\begin{aligned} \langle\bar{\eta}(z)| &= \langle\phi|(1 + G_0(z)t(z)) \\ &= \frac{1}{z - E_b}\langle\phi|(z - H_0)\ . \end{aligned} \tag{23}$$

Thus, the modified transition amplitude, in which the Pauli-forbidden state is projected to infinity becomes with $z \equiv E$,

$$\tilde{t}(E) = t(E) - (E - H_0)\frac{|\phi\rangle\langle\phi|}{E - E_b}(E - H_0). \tag{24}$$

This modified two-body transition amplitude can easily be implemented in the Faddeev equations as written in Eq. (9). Since different channels may have Pauli-forbidden states at different energies, in general, one has $E_b \equiv E_b(i)$. Although in this section we have dropped the explicit mention of the index i, Pauli-forbidden states in different subsystems can be implemented without any problem.

In case there are several Pauli-forbidden states in a specific channel of a subsystem, it is straightforward to generalize Eq. (24) to give

$$\tilde{t}(E) = t(E) - (E - H_0) \sum_b \frac{|\phi_b\rangle\langle\phi_b|}{E - E_b}(E - H_0), \tag{25}$$

where b runs over the number of Pauli-forbidden states.

Although the expression of Eq. (24) was presented in Ref. [18], it was not used in this form. Rather the Faddeev equations were modified to explicitly accommodate the two-body bound state being projected out. In fact, due to the difference $(E - H_0)$, where E is the energy of the subsystem and thus depending on the spectator momentum q, the expression of Eq. (24) is not a priori separable in the coordinates needed in the Eqs. (14). This makes the task of incorporating the Pauli projection into the separable expansion somewhat challenging.

To proceed, we first recall the basic properties of the generalized EST separable representation scheme [42]. The EST separable potential in any given partial wave has the form

$$v^{sep}(p', p) = \sum_{lm} h_l(p')\ \lambda_{lm}\ h_m(p), \tag{26}$$

where the form factors are given as the off-shell t matrices

$$h_l(p') \equiv t(p', p_l; E_l), \tag{27}$$

corresponding to the original potential V. The strength of the potential is represented by matrix elements λ_{lm} which depend entirely on the form factors. This implies that the potential $v^{sep}(p', p)$ is completely determined by the choice of form factors. According to Eq. (27), the latter are uniquely specified by the EST support points $\{E_l, p_l\}$, where E_l is a fixed energy and p_l a fixed momentum. We shall refer to E_l as the support energy and p_l the support momentum hereafter. The momentum p_l can either be on-shell or off-shell for positive values of E_l. For negative support energies, p_l is always off-shell. The number of EST support points give the rank of the separable expansion as well as the upper bound for the indices l and m. If the potential used to compute $t(p', p_l; E_l)$ supports a bound state, the latter will be present in the separable expansion. If this bound state is a Pauli forbidden state, we choose the potential $\tilde{V}$ defined in Eq. (15) as the starting point in the EST construction and the Pauli forbidden state is projected out. Constructing a separable expansion of $\tilde{V}$ implies that the form factors $h_l = t(p', p_l; E_l)$ in Eq. (26) are replaced by $\tilde{h}_l(p') = \tilde{t}(p', p_l; E_l)$. Additionally, the matrix elements λ_{lm} must be replaced by $\tilde{\lambda}_{lm}$, where the latter are computed using the form factors $\tilde{h}_l(p')$. Starting from Eq. (24) the expression for the modified form factors is given by

$$\tilde{h}_l(p') = h_l(p') - \frac{(E_l - E_{p'})}{(E_b - E_{p'})} h_b(p') \frac{1}{E_l - E_b} h_b(p_l) \frac{(E_l - E_{p_l})}{(E_b - E_{p_l})}, \tag{28}$$

where $h_b(p') \equiv \langle p'|V|\phi\rangle$. The momentum subscripts on the energy variables imply $E_{p_l} = 2\mu p_l^2$. The explicit derivation of Eq. (28) is given in Appendix B. Using $\tilde{h}(p)$ in the separable expansion is straightforward and does not increase the rank. Multiple Pauli forbidden bound states simply produce additional modifications to the form factors in accordance with Eq. (25).

III. RESULTS AND DISCUSSION

A. Interactions in the two-body subsystems

For computing the ground state of ^{6}Li in a three-body model, we need the interactions in the different subsystems, np, $n\alpha$, and $p\alpha$. For the np subsystem, we employ the CD-Bonn potential [43] and include only the deuteron channel ($^3S_1 - ^3D_1$). This potential is one of the so-called 'high-precision' potentials that fit the two-nucleon observables up to 300 MeV with $\chi^2 \approx 1$. The proton and neutron masses given in Ref. [43] are $m_p = 938.2723$ MeV and $m_n = 939.5656$ MeV. For the $n\alpha$ ($p\alpha$) subsystem, we ignore the microscopic structure of the alpha-particle and employ a phenomenological interaction that is fitted to the low-energy nucleon-alpha phase shifts. Here we include the $S_{1/2}$, $P_{1/2}$, and $P_{3/2}$ partial waves. Our choice is the interaction given by Bang [44], which is of Woods-Saxon

type, and supports a Pauli-forbidden S-wave bound state. For this work, we slightly modify the Bang potential by changing the central potential depth from -43 MeV to -44 MeV, to improve the description of the $n\alpha$ and $p\alpha$ phase shifts, particularly of the P-waves below $E_{lab} = 10$ MeV. As mass of the alpha particle we use $m_\alpha = 3727.379$ MeV. The S- and P-wave phase-shifts for $n + \alpha$ and $p + \alpha$ scattering calculated with this potential are shown in Fig. 1. They are compared to the phase shifts [45] extracted from an R-matrix fit to data.

To describe the $p\alpha$ interaction, we add to the $n\alpha$ potential a Coulomb force that consists of a short-range part, corresponding to a charged sphere of radius $R_c = 1.25 \times 4^{1/3}$ fm and the standard long-range point Coulomb force [33],

$$V_c(r) = \begin{cases} \frac{Z_1 Z_2 e^2}{2R_c}\left[3 - \left(\frac{r}{R_c}\right)^2\right] & r < R_c \\ \frac{Z_1 Z_2 e^2}{r} & r > R_c, \end{cases} \tag{29}$$

where $Z_1 Z_2 = 2$, and $e^2 = 1.43997$ MeVfm.

B. Binding energy of ^{6}Li: separable vs non-separable

In this section, we consider two approaches to solve the momentum-space Faddeev equations for the ground state of ^{6}Li using the two-body interactions described in Section III A as input. The first approach consists of solving the bound state Faddeev equations directly as given by Eqs. (9) leading to an 'exact' solution of the three-body bound state problem. The numerical results are obtained using Gauss-Legendre quadratures. The momentum grids for converged results consist of $N_p = 200$ points for the pair momentum p and $N_q = 200$ for the spectator momentum q. The maximum values for the above-mentioned momenta are set to $p = 60$ fm^{-1} and $q = 60$ fm^{-1}, respectively. This calculation yields $E_3 = -3.787$ MeV for the three-body binding energy of ^{6}Li when no Coulomb interaction is included and $E_3 = -2.777$ MeV with the Coulomb interaction of Eq. (29). The Coulomb potential is treated by introducing a cutoff radius R_{cut} beyond which $V_c(r)$ is set to zero. The momentum space representation is evaluated using either an analytic or numerical Fourier transform. Both methods are numerically stable. To further test the numerical stability of the calculation, the binding energy was computed using different values of the cutoff radius. We found that the result for E_3 is independent of the cutoff radius for $R_{cut} > 15$ fm. The experimental value is $E_3^{exp} = -3.699$ MeV from Ref. [46]. Our three-body calculation slightly underbinds ^{6}Li, a standard feature of these three-body models. The difference is typically accounted through a three-body interaction [47].

The second approach for solving the Faddeev equations consists of two steps. First, the EST [42] scheme is employed to construct separable representations of the two-body potentials given in Section III A. Then, the separable interactions are used to solve Eqs. (14) in order to obtain the three-body binding energy as well as the Faddeev amplitude according to Eq. (13). In the current example, the separable expansion is used to make a prediction for the ^{6}Li three-body binding energy with a precision of four significant figures. To check the accuracy of this prediction, the results are compared to the ones obtained directly without the separable expansion.

According to Eq. (27), the EST separable expansion employs solutions of the LSE as basis states. These states depend on two parameters, the two-body energy E_l as well as the asymptotic momentum p_l. We refer to each combination of E_l and p_l as an EST support point. It should be pointed out that if one employs the constraint $E_l = 2\mu p_l^2$, with μ being the reduced mass of the two-body system, the basis states depend only on one parameter. While the EST scheme [22, 29, 30] has been applied in solving Faddeev equations in separable form, those works did not take advantage of the full parameter space by imposing $p_l = \sqrt{2\mu|E_l|}$. We make use of the full parameter space for the basis states and choose p_l and E_l independently as suggested in Ref. [42]. The bound state Faddeev equations require off-shell two-body t-matrices as input in the energy range $-\infty \leq E_{2b} \leq E_3$. Therefore, a good separable representation of the off-shell properties of the t-matrices is required to reproduce the direct calculation accurately.

A successful application of the EST scheme hinges on an effective selection of the support energies and momenta. Since we are interested in a separable expansion for two-body energies E_{2b} between $-\infty$ and E_3, we restrict ourselves to negative energy support points. The off-shell t matrix has a smooth energy-dependence and is dominated by the energy-independent Born term at large values of $|E_{2b}|$. It is thus not necessary to incorporate support points at large negative energies. In practice, it is sufficient to consider support energies in the range -100 MeV $\leq E_l \leq 0$.

The use of separable expansions for the two-body potentials introduces uncertainty in three-body observables. This uncertainty must be quantified in order to make meaningful predictions. The dependence of E_3 on the choice of support points reflects the uncertainty in our procedure. By varying the latter while keeping the rank fixed can lead to a quantitative estimate of this uncertainty. Carrying out this procedure for successively increasing ranks provides means for making precise predictions of three-body observables using this approach.

Contrary to the smooth energy dependence of the off-shell t matrix, its dependence on the off-shell momenta is much more intricate and is determined by the shape of the underlying potential. As a consequence, the predicted

three-body observables show more sensitivity to the choice of the support momenta. To make an economic choice for the latter, we first identify the relevant range of the t matrix in momentum space and define the support momenta within it.

To illustrate how the support momenta are chosen, the off-shell t matrix corresponding to the CD-Bonn potential is computed for the ${}^3S_1 - {}^3D_1$ partial wave. Figure 2 shows the off-shell t matrix elements $t_{l_{np}'l_{np}}(p', p; E_{2b})$ for the np system as a function of the off-shell momentum p. The matrix elements $t_{00}(p', p; E_{2b})$ are depicted in panel (a) while $t_{22}(p', p; E)$ and $t_{20}(p', p; E)$ are shown in panels (b) and (c). The center-of-mass energy (c.m.) is fixed at $E_{2b} = -50$ MeV. Results obtained using the CD-Bonn potential are indicated by solid lines for $p' = 0.3$ fm^{-1} and dashed lines for $p' = 0.8$ fm^{-1}. Corresponding t matrix elements calculated using a rank-6 separable representation of the CD-Bonn potential are illustrated by triangles for $p' = 0.3$ fm^{-1} and diamonds for $p' = 0.8$ fm^{-1}. The energies are in units of MeV while the momenta are given in fm^{-1}. The support points are $\{E_l, p_l\} = \{-60, 0.4\}, \{-60, 1.1\}, \{-60, 2.5\}, \{-5, 0.4\}, \{-5, 1.1\}, \{-5, 2.5\}$. As mentioned above, the support energies are selected within the range -100 MeV $\leq E_l \leq 0$. Their specific values can be altered without compromising the accuracy of the separable representation. However, the support momenta are chosen to reproduce the structure of the t matrix below 5 fm^{-1}. As a first guess, the momenta are chosen such that there is one in the vicinity of each minimum or maximum. Improvement of the separable expansion is attained by further adjustment of the initial values.

The choice of momenta is not unique since a slight change in the given values can still capture the structure of the off-shell t matrix. However, changing the value of each support momentum by, e.g. 0.5 fm^{-1}, can already lead to a poor representation of the t matrix, as well as the three-body observables. It is thus imperative to check that each chosen set of momenta captures the shape of the off-shell t matrix in order to ensure that the separable expansion converges rapidly. It should be noted that, although the structure of the t matrix differs for each E and p', the regions of intricate momentum dependence remain mostly unaltered. For example, this can be seen by comparing the t matrix at $p' = 0.3$ fm^{-1} and $p' = 0.8$ fm^{-1}. Although the shape is quite different in each case, the features that determine the location of the support momenta are situated at similar positions. Consequently, the support points adjusted to reproduce the off-shell t matrix at $p' = 0.3$ fm^{-1} are equally well suited for $p' = 0.8$ fm^{-1}. Thus, by accurately representing the off-shell t matrix at a single energy by including several support momenta, one can obtain an accurate representation of the off-shell t matrix at other energies. Although such a choice is specific to the CD-Bonn potential, these support points would be applicable to any NN t matrix that exhibits either (1) a similar off-shell structure or (2) a considerably less complicated dependence on the off-shell momenta. The structure of the NN t matrix corresponding to most high precision and chiral potentials is similar in the low momentum region that determines the support momenta. We thus expect that the support points determined for the CD-Bonn potential will provide an equally good representation for all such NN potentials. For example, we verified that those same support points yield excellent results for the high precision Nijmegen I [48] and AV18 [49] as well as the chiral potential of Ref. [50]. Contrarily, the structure of the off-shell t matrix corresponding to the Woods-Saxon Bang potential is very different from that of the NN t matrices, and thus an independent determination of the support momenta must be carried out.

To quantify the uncertainty on the three-body binding energy, separable representations of successively increasing rank are constructed for both, the CD-Bonn and the Bang potential. Table I shows several separable representations of the CD-Bonn potential. The first and second columns give the label and rank of the separable potential. The EST support energies and momenta are listed in the third and forth columns, respectively. The same information is given in Table II for the Bang potential. To proceed, we first fix the EST support points for the Bang interaction while varying those of the CD-Bonn potential. Table III shows the three-body binding energies for the ground state of ^{6}Li calculated using a variety of np separable representations taken from Table I. For this study we do not include the Coulomb interaction. The EST8-4 separable representation of the Bang interaction defined in Table II is adopted in the $n\alpha$ and $p\alpha$ subsystems. To ease comparison, we include in the last rows of Tables III and IV the exact results obtained when solving Eq. (9) directly.

We observe that the numerical value for the binding energy fluctuates as the support points are varied. However, the fluctuations decrease as the rank of the separable potentials is increased. From Table III we see that the uncertainty in the binding energy is $\delta E_3 \approx 50$ keV for the rank 3 representation. Increasing the rank to five reduces the uncertainty down to $\delta E_3 \approx 5$ keV. A further increase of the rank to six reduces the uncertainty to $\delta E_3 \approx 0.5$ keV, which corresponds to a precision of four significant figures. In addition to the uncertainty associated with the selection of the support energies, one must take into account the convergence of the binding energy with respect to the rank of the separable potential. From Table III we see that increasing the rank from six to seven leaves the fourth digit of the binding energy unaltered. This observation, together with the fact that $\delta E_3 < 0.5$ keV, guarantees that the numerical result for E_3 is precise to four significant figures.

Next, the support points for the CD-Bonn potential are fixed and those corresponding to the Bang potential are varied. Table IV is the same as Table III but shows results for different separable expansions of the Bang interaction.

The EST8-1 separable representation of the CD-Bonn potential taken from Table I is adopted for the np subsystem. Here we observe that rank-3 and rank-4 potentials lead to the uncertainties $\delta E_{3b} \approx 40$ keV and $\delta E_{3b} \approx 13$ keV. Moreover, a rank-7 representation is needed in order to obtain an uncertainty of approximately 0.5 keV. To ensure that the binding energy is converged to at least four significant figures, it is necessary to increase the rank to 8. The predicted value for the three-body binding energy can thus be read off from Tables III and IV as $E_{3b} = -3.787$ MeV, in perfect agreement with the exact result.

The rapid reduction of the uncertainty observed in Tables III and IV is primarily due to the efficient choice of the support momenta. To illustrate this point, we consider calculations in which the constraint $p_l = \sqrt{2\mu|E_l|}$ is imposed. We choose three sets of support support energies for the CD-Bonn potential, namely, $E_l = [-150, -120, -80, -60, -45, -35, -15, -5\}$ MeV, $\{-180, -140, -100, -70, -55, -35, -10, -3\}$ MeV, and $\{-200, -160, -120, -80, -40, -25, -10, -4\}$ MeV. These sets yield $E_{3b} = -3.803$ MeV, $E_{3b} = -3.788$ MeV, and $E_{3b} = -3.795$ MeV, respectively. Here we see that despite being rank-8, these representations lead to fluctuations in the third digit. This demonstrates that, in order to obtain a result that is precise to four significant figures, it is essential that the full parameter space for choosing a basis is considered and the support momenta are chosen independently from the support energies.

Finally we calculate the three-body binding energy of ^{6}Li when the Coulomb interaction of Eq. (29) is included in the description of the $p\alpha$ subsystem. The Coulomb interaction leads to a different structure of the the $p\alpha$ potential, and the above analysis has to be repeated, leading to a different set of support points. The rank required to obtain a precision of at least four significant figures remains unchanged at eight. Using a rank-8 separable representations for the Coulomb and Bang potentials yields a three-body binding energy of -2.777 MeV which agrees completely with the exact calculation. The support points were chosen to be $\{E_l,\ p_l\}$ = {-55,0.2}, {-55,1.0}, {-55,1.2}, {-55,3.0}, {-3,0.2}, {-3,1.0}, {-3,1.2}, {-3,3.0}.

Lastly, we want to comment that it is mandatory to perform the projection procedure for the Pauli-forbidden state in the separable representation as in the exact calculation.

C. Properties of ^{6}Li

After discussing the convergence and accuracy of the three body binding energy of ^{6}Li, we need to consider properties of the wave function obtained in both schemes, since we do not only want to have excellent agreement in the three-body binding energy but also in observables derived from the wave function. To this aim, we consider the momentum distributions with respect to the Jacobi coordinates of the wave function $\Psi(\vec{p}, \vec{q})$. Choosing a specific set of Jacobi variables, e.g. the set $(ij)k$, in which k is the spectator with respect to the pair (ij), the momentum distribution of the spectator is given as

$$n(q_k) = \sum_{\alpha_k} \int dp_k p_k^2 |\Psi_{\alpha_k}(p_k, q_k)|^2, \tag{30}$$

and the momentum distribution of the pair is given as

$$n(p_k) = \sum_{\alpha_k} \int dq_k q_k^2 |\Psi_{\alpha_k}(p_k, q_k)|^2. \tag{31}$$

The momentum distribution of the different pairs in the ground state of ^{6}Li are shown in panels (a) and (b) of Fig. 3 on a linear as well as a logarithmic scale, where the corresponding pair is indicated in the round brackets of the legend. The solid, dashed as well as dotted lines are calculated using the non-separable forces, whereas the crosses, downward and upward triangles correspond to the same calculation using separable forces. The calculations are in excellent agreement. For small momenta, the distribution in the (np) pair is about twice as large as the ones in the $(n\alpha)$ and $(p\alpha)$ pairs, whereas for momenta larger than 2 fm^{-1} there is an order of magnitude (or more) difference between the momentum distribution in the (np) pair and the $(n\alpha)$ and $(p\alpha)$ pairs, an indication of the high momentum components of the CD-Bonn potential.

Panels (c) and (d) of Fig. 3 depict the momentum distributions of the spectator particle with respect the pair given in brackets in the legend. For very small momenta q, the distribution of the alpha momentum with respect to the (np) pair dominates by an order of magnitude over the ones of the two other spectator momenta. However, the logarithmic scale in panel (d) shows that for different values of q, these roles interchange twice. Finally, for $q \geq 3.5$ fm^{-1} the distributions in which either the proton or the neutron are the spectators dominate, which, again is a reflection of the high momentum components of the CD-Bonn potential.

As discussed in Sec. III A, the effective interaction between the neutron (proton) and the alpha particle is represented by Woods-Saxon type potentials. Thus, in both subsystems there is a bound state in the $S_{1/2}$-state, for the $n\alpha$

subsystem this bound state is at -10.326 MeV and for the $p\alpha$ subsystem at -8.879 MeV. Those bound states are forbidden by the Pauli principle, and need to be projected out using the formulation outlined in Sec. II B. In both subsystems we introduce an additional term to the potential according to Eq. (15), $\hat{V}^i = \lambda_i |\phi^i\rangle\langle\phi^i|$, and let the parameters λ_i go to infinity.

In order to better understand the action of the parameters $\lambda_{n\alpha} = \lambda_{p\alpha} \equiv \lambda$, we choose a set of finite values for λ and calculate the ground state three-body binding energy and expectation value as function of λ. The results of these calculations are listed in Table V. To simplify this study, the Coulomb potential is here omitted, leading to $V_{n\alpha} = V_{p\alpha}$. The expectation value of the total Hamiltonian is in this case given by

$$\begin{aligned} \langle E_3(\lambda)\rangle &\equiv \langle\Psi(\lambda)|H_{3b}|\Psi(\lambda)\rangle \\ &= \langle\Psi(\lambda)|H_0 + V_{np} + 2V_{n\alpha}|\Psi(\lambda)\rangle, \end{aligned} \tag{32}$$

where H_{3b} is the three-body Hamiltonian. The values of $E_3(\lambda)$ obtained from the solution of the Faddeev equation, Eq. (9), start to agree with the expectation value calculated using Eq. (32) within 4 significant figures once λ exceeds 1000 fm^{-1}. Letting $\lambda \to \infty$ gives perfect agreement. In order to illustrate that the Pauli forbidden $S_{1/2}$ state $|\phi_{n\alpha}\rangle$ is completely projected out for $\lambda \to \infty$, we define a probability

$$\mathcal{P}_{TDB}(\lambda) = \sum_{\alpha'_k} \int_0^\infty q_k^2 \left| \int_0^\infty dp'_k \; {p'_k}^2 \; \phi_{\alpha'_k}(p'_k) \Psi_{\alpha'_k}(p'_k, q_k; \lambda) \right|^2 dq_k, \tag{33}$$

which gives the overlap between the Pauli forbidden $S_{1/2}$ state and the ^{6}Li ground state wave function calculated for a specific λ. A detailed discussion of this probability is provided in Appendix C. Obviously, this quantity is calculated in the Jacobi coordinates where $n\alpha$ constitutes the subsystem. The calculated values of $\mathcal{P}_{TDB}(\lambda)$ are listed in the last column of Table V and clearly indicate that for $\lambda \geq 10^4$ fm^{-1} the overlap is numerically zero.

Studying the evolution of the three-body binding energy as function of the parameter λ shows how the deep three-body bound state including the Pauli forbidden states in the $n\alpha$ and $p\alpha$ subsystems moves to the physical three-body bound state. However, the binding energy does not give further information about the characteristics of the bound state. Since the Pauli forbidden states in the $n\alpha$ and $p\alpha$ subsystems occur in the $S_{1/2}$ partial wave, the unphysical deep bound state should be dominated by this partial wave. However, we know that the physical ground state is dominated by $P_{3/2}$ components. It is thus illustrative to investigate how the components of the ground state wave function change as a function of the parameter λ. To proceed, we note that the probability for each partial wave state $|\alpha_k\rangle$ in the three body wavefunction is given by

$$\langle\Psi_{\alpha_k}(\lambda)|\Psi_{\alpha_k}(\lambda)\rangle = \int_0^\infty dp_k \; dq_k \; p_k^2 q_k^2 \; \left|\Psi_{\alpha_k}(p_k, q_k; \lambda)\right|^2. \tag{34}$$

Here the index k represents the Jacobi coordinate $(n\alpha)p$ in which the proton is the spectator with momentum q_k. We recall that the three-body angular momentum states $|\alpha_k\rangle$ are constructed by coupling angular momentum states of the pair $|\beta_k\rangle$ to those of the spectator $|\gamma_k\rangle$, so that $|\alpha_k\rangle = |\beta_k\rangle \otimes |\gamma_k\rangle$. In the present case $|\beta_k\rangle$ corresponds to the $S_{1/2}$, $P_{1/2}$, and $P_{3/2}$ partial wave states of the $n\alpha$ subsystem. To determine the probability for each of those two-body states, one must sum over the angular momenta of the spectator γ_k. The probability for a state $|\beta_k\rangle$ is thus given by

$$N_\beta(\lambda) = \sum_\gamma \int_0^\infty dp \; dq \; p^2 q^2 \; \left|\Psi_\alpha(p, q; \lambda)\right|^2, \tag{35}$$

where $\alpha = \{\beta, \gamma\}$ and the subscript k is omitted for concision. Figure 4 shows the values of $N_\beta(\lambda)$ as a function of λ for the ^{6}Li three-body ground state. The solid, dashed, and dot-dashed lines represent the $S_{1/2}$, $P_{3/2}$ and $P_{1/2}$ partial wave states of the $n\alpha$ subsystem. The vertical line indicates the value of λ for which the $n\alpha$ system becomes unbound. As expected, for $\lambda = 0$ the ground state is completely dominated by the $S_{1/2}$ state. This remains true for values of λ smaller than 0.05 fm^{-1}. It is worthwhile to note that, even when the $n\alpha$ subsystem becomes unbound, the three-body ground state of ^{6}Li is still dominated by the $S_{1/2}$ component. Only when λ approaches 0.1 fm^{-1}, the probability of the $S_{1/2}$ component rapidly decreases. The corresponding probability of the $P_{3/2}$ rapidly increases to its final value of about 70%. Moreover, the ground state acquires a $P_{1/2}$ probability of about 20% and maintains an $S_{1/2}$ probability of about 10% which is due to the continuum states of $n\alpha$, $p\alpha$, and np subsystems.

IV. SUMMARY AND OUTLOOK

In this work, we explore solving momentum-space Faddeev equations using separable interactions based on the EST scheme [26–28], for bound three-body systems of the type $n+p+A$. Our goal is to benchmark this separable method against the standard approach of directly solving momentum-space Faddeev equations. We apply both approaches to ^{6}Li, taking the CD-Bonn [43] interaction for the np pair and the Bang [44] potential for the $n(p)$-α subsystems. Our results for the ^{6}Li bound state demonstrate that using a separable implementation of the Faddeev equations is equivalent to solving them directly: the binding energies obtained with the separable interactions agree within 4-digits with the exact calculation, and the momentum distributions are also in perfect agreement. Our values of the binding energy obtained for ^{6}Li with CD-Bonn and Bang are consistent with previous three-body calculations. Since we are dealing with a bound state problem, including the Coulomb interaction in the momentum-space Faddeev equations does not present a problem in both approaches.

As a consequence of our study, there are a few important developments worth highlighting. First and foremost, we extended the EST construction of the separable interaction to include off-shell properties of the t-matrix by allowing energy and momentum support points to be chosen independently. This proved to be critical for the high quality description of the properties of the three-body system and to achieve the desired 4-digit precision. Second, the energy and momentum support points developed for the np subsystem are independent of the choice of the NN interaction as long as it describes the low energy behavior of the deuteron channel with high precision. The numerical implementation valid for the CD-Bonn interaction will transport immediately to other high precision NN potentials as well as chiral NN potentials. However, when solving the $n+p+A$ problem for bound systems where $A > 4$, and given the wide range of nucleon-nucleus effective interactions available, we expect one will need to inspect the properties of the two-body nucleon-nucleus t-matrices carefully and revisit the issue of optimum energy and momentum support points in those cases again. Similar to [26–28], we find here that the structure of the two-body t-matrices as a function of energy and momentum determines the minimal rank needed for an accurate description of both the two-body and three-body observables.

Another important development resulting from this study concerns the method used to project two-body Pauli-forbidden states out of the model space. We have developed an approach that does not modify the Faddeev equations and thus can be implemented straightforwardly in momentum-space Faddeev equations either in their non-separable or EST-type separable representation. This approach is effective in projecting out the forbidden state at a minimal computational cost. We also provide a generalization for dealing with an arbitrary number of Pauli-forbidden states in a computationally efficient manner. This will be essential when moving to heavy systems.

This work lays the ground to now proceed to three-body scattering with EST-separable interactions. In the separable formulation, the Coulomb interaction can be accurately taken into account even for complex nuclei with large Z as outline in Ref. [16]. The next step is to tackle $d + A$ elastic scattering below and above the three-body breakup threshold, followed by the ultimate goal of applying the method to deuteron induced nuclear reactions on heavy ions, at energies well above three-body breakup threshold.

Appendix A: Explicit representation of non-separable and separable Faddeev equations

Here we summarize the explicit expressions entering our formulation of the Faddeev Eqs. (9) and (14). Besides the t-matrix, the Faddeev equations in non-separable form require coordinate transformations from Jacobi momenta that single out particle i to Jacobi coordinates that single out particle k. These are most conveniently performed separately for orbital and spin space. Therefore, the basis states of Eq. (7) are first recoupled into an LS basis and then the transformation is applied. The resulting geometrical function is then

$$\begin{aligned}\mathcal{G}_{\alpha_k\alpha_i}(p_kq_kx) = &\sum_{LS}(2S+1)\sqrt{(2J_{ij}+1)(2J_k+1)(2J_{jk}+1)(2J_i+1)}\left\{\begin{array}{ccc} l_k & s_k & J_{ij}\\ \lambda_k & j_k & J_k\\ L & S & J\end{array}\right\}\left\{\begin{array}{ccc} l_i & s_i & J_{jk}\\ \lambda_i & j_i & J_i\\ L & S & J\end{array}\right\}\\ &\times 8\pi^2\sum_{M=-L}^{L}\left\{Y^*_{l_k}(\hat{p}_k)\,Y^*_{\lambda_k}(\hat{q}_k)\right\}^{LM}\left\{Y_{l_i}(\widehat{-\alpha\vec{p}_k-\beta\vec{q}_k})\,Y_{\lambda_i}(\widehat{\vec{p}_k-\gamma\vec{q}_k})\right\}^{LM}\\ &\times(-)^{s_i+2j_i+j_j+j_k}\sqrt{(2s_k+1)(2s_i+1)}\left\{\begin{array}{ccc} j_i & j_j & s_k\\ j_k & S & s_i\end{array}\right\}\quad . \end{aligned} \tag{A1}$$

The spherical harmonics $Y_{lm}(\hat{p})$ dependent on the angles $\hat{p}$ of the vector $\vec{p}$. For the evaluation, we choose a coordinate system where the pair momentum is angular independent and the spectator momentum is in the x-y plane:

$$\vec{p}_k=\begin{pmatrix}0\\0\\p_k\end{pmatrix}\qquad \vec{q}_k=\begin{pmatrix}q_k\sqrt{1-x^2}\\0\\q_kx\end{pmatrix}\quad . \tag{A2}$$

The curly brackets grouping the spherical harmonics indicate that they are coupled to a state of total orbital angular momentum L and third component M. The mass ratios are given by

$$\begin{aligned}\alpha &= \frac{m_k}{m_j+m_k}\\ \beta &= \frac{(m_i+m_j+m_k)\,m_j}{(m_i+m_j)(m_j+m_k)}\\ \gamma &= \frac{m_i}{m_i+m_j}\quad .\end{aligned} \tag{A3}$$

For this case, the shifted momenta are given by

$$\begin{aligned}\pi'_i(p_kq_kx) &= \sqrt{\alpha^2p_k^2+\beta^2q_k^2+2\alpha\beta p_kq_kx}\\ \chi'_i(p_kq_kx) &= \sqrt{p_k^2+\gamma^2q_k^2-2\gamma p_kq_kx}\quad .\end{aligned} \tag{A4}$$

For the derivation, we followed similar steps as in Ref. [34]. Different but equivalent expressions that involve Legendre polynomials can be derived [51]. We used the ones given above since the numerical implementation is stable even for large orbital angular momenta.

For the derivation of Eq. (14), we insert the separable expansion Eq. (13) into the Faddeev equations. It is then advantageous to substitute the p'_k integral by an integral over q_i or q_j, respectively. The Faddeev equations then read

$$\begin{aligned}\psi_k^{\alpha_k}(p_k,q_k) = G_0(E_{q_k},p_k)\sum_{\alpha'_k}\int_{-1}^{1}dx\Bigg[&\int dq_iq_i^2t_k^{\alpha_k\alpha'_k}(p_k,\pi_k;E_{q_k})\sum_{\alpha'_i}\tilde{\mathcal{G}}_{\alpha'_k\alpha'_i}(q_kq_ix)\psi_i^{\alpha'_i}(\pi'_i,q_i)\\ &+\int dq_jq_j^2t_k^{\alpha_k\alpha'_k}(p_k,\pi_k;E_{q_k})\sum_{\alpha'_j}\tilde{\mathcal{G}}_{\alpha'_k\alpha'_j}(q_kq_jx)\psi_j^{\alpha'_j}(\pi'_j,q_j)\Bigg]\quad .\end{aligned} \tag{A5}$$

In this case, the geometrical function is defined by

$$\tilde{\mathcal{G}}_{\alpha_k\alpha_i}(q_kq_ix) = \sum_{LS}(2S+1)\sqrt{(2J_{ij}+1)(2J_k+1)(2J_{jk}+1)(2J_i+1)}\left\{\begin{array}{ccc} l_k & s_k & J_{ij} \\ \lambda_k & j_k & J_k \\ L & S & J \end{array}\right\}\left\{\begin{array}{ccc} l_i & s_i & J_{jk} \\ \lambda_i & j_i & J_i \\ L & S & J \end{array}\right\}$$
$$\times 8\pi^2 \sum_{M=-L}^{L}\left\{Y^*_{l_k}(\widehat{\gamma\vec{q}_k+\vec{q}_i})\,Y^*_{\lambda_k}(\hat{q}_k)\right\}^{LM}\left\{Y_{l_i}(\widehat{-\vec{q}_k-\alpha\vec{q}_i})\,Y_{\lambda_i}(\hat{q}_i)\right\}^{LM}$$
$$\times(-)^{s_i+2j_i+j_j+j_k}\sqrt{(2s_k+1)(2s_i+1)}\left\{\begin{array}{ccc} j_i & j_j & s_k \\ j_k & S & s_i \end{array}\right\} \quad . \tag{A6}$$

The momentum vectors are chosen as

$$\vec{q}_k = \begin{pmatrix} 0 \\ 0 \\ q_k \end{pmatrix} \qquad \vec{q}_i = \begin{pmatrix} q_i\sqrt{1-x^2} \\ 0 \\ q_ix \end{pmatrix}, \tag{A7}$$

and the shifted momenta change to

$$\pi_k(q_kq_ix) = \sqrt{\gamma^2q_k^2+q_i^2+2\gamma q_kq_ix}, \tag{A8}$$
$$\pi'_i(q_kq_ix) = \sqrt{q_k^2+\alpha^2q_i^2+2\alpha q_kq_ix}.$$

Using this form of the Faddeev equations, it is easy to read off Eq. (14). Since the form factors of the separable interaction are given a priori, it is possible to precalculate the angular integral leading to the definition

$$Z^{(ki)}_{n\alpha_k,\nu\alpha_i}(q_k,q_i) = \int_{-1}^{1} dx\; h^{\alpha_k}_n(\pi_k)\tilde{\mathcal{G}}_{\alpha_k\alpha_i}(q_kq_ix)G_0(E_{q_i},\pi'_i)h^{\alpha_i}_\nu(\pi'_i) \quad . \tag{A9}$$

The wave functions cannot be represented in a separable form. They are obtained from $\psi^{\alpha_k}_k(p_k,q_k)$ using Eq.(2). Thereby further coordinate transformations using either $\mathcal{G}_{\alpha_k\alpha_i}(p_kq_kx)$ or $\tilde{\mathcal{G}}_{\alpha_k\alpha_i}(q_kq_ix)$ are required to represent all three Faddeev components in the same set of coordinates.

Appendix B: Projecting Pauli-forbidden states in case of separable potentials

In order to set up the formulation for projecting a Pauli-forbidden state to infinity when using separable potentials based in the EST formulation, let us have a closer look at the functions $|\eta(z)\rangle$ and $\langle\bar{\eta}(z)|$ of Eqs. (21). The explicit momentum space representation reads

$$\begin{aligned}\langle\bar{\eta}(z)|p\rangle &= \langle\phi|\big[1+G_0(z)t(z)\big]|p\rangle \\ &= \langle\phi|G(z)G_0(z)^{-1}|p\rangle \\ &= \frac{z-E_p}{z-E_b}\langle\phi|p\rangle \\ &= \frac{z-E_p}{z-E_b}\langle\phi|VG_0(E_b)|p\rangle \\ &= \frac{z-E_p}{z-E_b}\langle\phi|V|p\rangle\frac{1}{E_b-E_p},\end{aligned} \tag{B1}$$

where we used the Schrödinger equation for $\langle\phi|p\rangle$. The momentum subscript, p, on the energy variable, E, implies $E_p = p^2/2\mu$, while the bound state energy is represented by E_b. Similarly, one obtains

$$\begin{aligned}\langle p'|\eta(z)\rangle &= \langle p'|\big[1+t(z)G_0(z)\big]|\phi\rangle \\ &= \frac{1}{E_b-E_{p'}}\langle p'|V|\phi\rangle\frac{z-E_{p'}}{z-E_b}\,.\end{aligned} \tag{B2}$$

Putting everything together and setting $z\equiv E$, Eq. (24) takes the explicit form

$$\tilde{t}(p',p;E) = t(p',p;E) - \frac{(E-E_{p'})}{(E_b-E_{p'})}\,\frac{(E-E_p)}{(E_b-E_p)}\,\frac{\langle p'|V|\phi\rangle\langle\phi|V|p\rangle}{E-E_b}. \tag{B3}$$

The above expression clearly shows that the half-shell elements of $\tilde{t}(p',p;E)$ and $t(p',p;E)$ are identical, and for $E \to E_b$ the pole of t is removed for $\tilde{t}$. However, due to the differences $(E-E_{p'})$ and $(E-E_p)$, and having in mind that energy E of the subsystem depends on the spectator momentum q in the Faddeev equations, $\tilde{t}(p',p;E)$ is not yet in the separable form needed in Eqs. (14). At a specific off-shell support energy E_l and support momentum p_l we have

$$\tilde{t}(p',p_l;E_l) = t(p',p_l;E_l) - \frac{(E_l-E_{p'})}{(E_b-E_{p'})}\,\frac{\langle p'|V|\phi\rangle\langle\phi|V|p_l\rangle}{E_l-E_b}\,\frac{(E_l-E_{p_l})}{(E_b-E_{p_l})}, \tag{B4}$$

having in mind that these off-shell EST functions are characterized by $\{E_l,p_l\}$, and only need to be linearly independent and solutions of a Lippmann-Schwinger type integral equation [42]. The form factors that take into account the projection of the Pauli-forbidden state to infinity read,

$$\langle p'|\tilde{t}(E_l)|p_l\rangle \equiv \tilde{h}_{E_l,p_l}(p') = h_l(p') - \frac{(E_l-E_{p'})}{(E_b-E_{p'})}h_b(p')\frac{1}{E_l-E_b}h_b(p_l)\frac{(E_l-E_{p_l})}{(E_b-E_{p_l})}, \tag{B5}$$

where $h_l(p') \equiv t(p',p_l;E_l)$ and $h_b(p') \equiv \langle p'|V|\phi\rangle$. These form factors also define the strength constants λ_{nm} [42].

Appendix C: Probability of the Pauli Forbidden State in the ^{6}Li Ground State Wavefunction

The Pauli projection method described in Section II B shifts the energy of the forbidden two-body bound state to positive infinity. To estimate the probability of the Pauli-forbidden state in the ^{6}Li ground state three-body wavefunction, one needs to project it onto the subspace comprising of product states between the bound $n\alpha$ pair and the spectator nucleon. The two-body projector $P_\phi^{2b} = |\phi_\beta^{j_p}\,\beta\; j_p m_j\rangle\langle\phi_\beta^{j_p}\,\beta\; j_p m_j|$ is defined for that purpose, where the two-body bound state is characterized by the total pair angular momentum j_p and its projection along the z-axis m_j. The index β represents the spins and orbital angular momenta of the pair which couple to j_p separating different angular momentum components of the two-body bound state. Since P_ϕ^{2b} is defined in the two-body subspace, its application in the three-body space requires summation over the spectator quantum numbers as well as an integration over the spectator momentum. The projection operator in the three-body space thus takes the form

$$P_\phi = \sum_\beta \sum_{sm_sm_j} \int d\vec{q}\,\big|\vec{q}\;sm_s\;\phi_\beta^{j_p}\;\beta\;j_p m_j\big\rangle\,\big\langle\vec{q}\;sm_s\;\phi_\beta^{j_p}\;\beta\;j_p m_j\big|, \tag{C1}$$

where s is the spin of the spectator with m_s being its projection along the z-axis. The spectator momentum is denoted by $\vec{q}$. Since we are using a partial wave expansion to represent the three-body system, it is advantageous to represent the spectator in terms of partial wave states $|q(\lambda s)\mathcal{J}m_\mathcal{J}\rangle$. The angular dependence is expanded in terms of a spectator orbital angular momentum λ which is coupled with the spectator spin s to a total spectator angular momentum $\mathcal{J}$ and its third component $m_\mathcal{J}$. Finally, we couple the spectator and two-body bound state angular momenta to the total three-body angular momentum J and its third component M. In terms of these states, the projector can be rewritten as

$$P_\phi = \sum_\beta \sum_{\lambda s\mathcal{J}JM} \int_0^\infty dq\; q^2\big|q(j_p(\lambda s)\mathcal{J})JM\;\phi_\beta^{j_p}\;\beta\;\big\rangle\,\big\langle q(j_p(\lambda s)\mathcal{J})JM\;\phi_\beta^{j_p}\;\beta\;\big|, \tag{C2}$$

The sum over the angular momentum quantum numbers β, λ, s, $\mathcal{J}$, J and M and the integral over q implies that all possible configurations the spectator and the bound pair are included. Applying P_ϕ to the three body wavefunction yields

$$|\Psi^P\rangle \equiv P_\phi|\Psi^{JM}\rangle. \tag{C3}$$

From Eq. (C3) we see that the probability of the state $\big|\phi_\beta^{j_p}\;\beta\;j_p m_j\big\rangle$ is given by

$$\begin{aligned}\mathcal{P}_{TDB} &= \|\Psi^P\|^2 \\ &= \big\langle\Psi^{JM}\big|P_\phi^\dagger\;P_\phi\big|\Psi^{JM}\big\rangle.\end{aligned} \tag{C4}$$

Since P_ϕ is Hermitian and fulfills $P_\phi^2 = P_\phi$, the probability can be recast as the expectation value

$$\mathcal{P}_{TDB} = \big\langle\Psi^{JM}\big|\;P_\phi\big|\Psi^{JM}\big\rangle,$$

$$= \sum_{\beta} \sum_{\lambda s \mathcal{J} JM} \int_0^\infty dq\ q^2 \big\langle \Psi^{JM} \big| q(j_p(\lambda s)\mathcal{J}) JM\ \phi_\beta^{j_p}\ \beta\ \big\rangle\ \big\langle q(j_p(\lambda s)\mathcal{J}) JM\ \phi_\beta^{j_p}\ \beta\ \big| \Psi^{JM} \big\rangle \tag{C5}$$

To evaluate the quantity $\big\langle q(j_p(\lambda s)\mathcal{J}) JM\ \phi_\beta^{j_p}\ \beta\ \big| \Psi^{JM} \big\rangle$ we insert a complete set of momentum eigenstates

$$\big\langle q(j_p(\lambda s)\mathcal{J}) JM\ \phi_\beta^{j_p}\ \beta\ \big| \Psi^{JM} \big\rangle = \sum_{\alpha'} \int_0^\infty dp' p'^2\ dq' q'^2 \big\langle q(j_p(\lambda s)\mathcal{J}) JM\ \phi_\beta^{j_p}\ \beta\ \big| p' q' \alpha' JM \big\rangle \big\langle p' q' \alpha' JM \big| \Psi^{JM} \big\rangle,$$

$$= \int_0^\infty dp' p'^2\ \phi_\beta^{j_p}(p')\ \Psi_\alpha^J(p'q'). \tag{C6}$$

In the last step, we used that the quantum numbers of the projector agree with the definition of α' and therefore uniquely define all quantum numbers. The wave functions are independent of the third component and the magnitude of the spectator momentum is fixed by the projector, too. Based on this result, the desired probability is

$$\begin{aligned} \mathcal{P}_{TDB} &= \big\langle \Psi^{JM} \big|\ P_\phi \big| \Psi^{JM} \big\rangle, \\ &= \sum_{\alpha} \int_0^\infty dq\ q^2 \left| \int_0^\infty dp' p'^2\ \phi_\beta^{j_p}(p')\ \Psi_\alpha^J(p'q') \right|^2 \end{aligned} \tag{C7}$$

where α is short hand notation for β and λ, s, $\mathcal{J}$, J and M as defined in Eq. (7) in agreement with Eq. (33).

ACKNOWLEDGMENTS

This work was performed in part under the auspices of the National Science Foundation under contract NSF-PHY-1520972 with Ohio University and NSF-PHY-1520929 with Michigan State University, of the U. S. Department of Energy under contract No. DE-FG02-93ER40756 with Ohio University, and of DFG and NSFC through funds provided to the Sino-German CRC 110 "Symmetries and the Emergence of Structure in QCD" (NSFC Grant No. 11621131001, DFG Grant No. TRR110). A.N. acknowledges support of Ohio University through the Robert and René Glidden Visiting Professorship Program, and the Institute of Nuclear and Particle Physics and the Department of Physics and Astronomy. The authors thank J. Haidenbauer for constructive comments on the manuscript and D.R. Phillips for illuminating discussions while working on the manuscript. Part of the numerical computations have been performed on JUQUEEN and JURECA of the JSC, Jülich, Germany. This research also used resources of the National Energy Research Scientific Computing Center, a DOE Office of Science User Facility supported by the Office of Science of the U.S. Department of Energy under contract No. DE-AC02-05CH11231.

[1] J. Cizewski *et al.*, J. Phys. Conf **420**, 012058 (2013).
[2] R. Kozub, G. Arbanas, A. Adekola, D. Bardayan, J. Blackmon, *et al.*, Phys.Rev.Lett. **109**, 172501 (2012).
[3] J. E. Escher, J. T. Burke, F. S. Dietrich, N. D. Scielzo, I. J. Thompson, and W. Younes, Rev. Mod. Phys. **84**, 353 (2012).
[4] G. Potel *et al.*, Eur. Phys. J. **A53**, 178 (2017).
[5] S. D. Pain, D. W. Bardayan, J. C. Blackmon, S. M. Brown, K. Y. Chae, K. A. Chipps, J. A. Cizewski, K. L. Jones, R. L. Kozub, J. F. Liang, C. Matei, M. Matos, B. H. Moazen, C. D. Nesaraja, J. Okołowicz, P. D. O'Malley, W. A. Peters, S. T. Pittman, M. Płoszajczak, K. T. Schmitt, J. F. Shriner, D. Shapira, M. S. Smith, D. W. Stracener, and G. L. Wilson, Phys. Rev. Lett. **114**, 212501 (2015).
[6] K. T. Schmitt, K. L. Jones, A. Bey, S. Ahn, D. Bardayan, *et al.*, Phys.Rev.Lett. **108**, 192701 (2012).
[7] K. L. Jones, F. M. Nunes, A. Adekola, D. Bardayan, J. Blackmon, *et al.*, Phys.Rev. **C84**, 034601 (2011).
[8] A. Deltuva, Phys. Rev. C **88**, 011601 (2013).
[9] R. Varner, W. Thompson, T. McAbee, E. Ludwig, and T. Clegg, Phys.Rept. **201**, 57 (1991).
[10] S. Weppner, R. Penney, G. Diffendale, and G. Vittorini, Phys.Rev. **C80**, 034608 (2009).
[11] A. Koning and J. Delaroche, Nucl.Phys. **A713**, 231 (2003).
[12] A. Deltuva and A. Fonseca, Phys.Rev. **C79**, 014606 (2009).
[13] A. Deltuva, Phys.Rev. **C79**, 054603 (2009).

[14] F. M. Nunes and A. Deltuva, Phys.Rev. **C84**, 034607 (2011).
[15] N. J. Upadhyay, A. Deltuva, and F. M. Nunes, Phys.Rev. **C85**, 054621 (2012), arXiv:1112.5338 [nucl-th].
[16] A. Mukhamedzhanov, V. Eremenko, and A. Sattarov, Phys.Rev. **C86**, 034001 (2012).
[17] A. Eskandarian and I. R. Afnan, Phys. Rev. **C46**, 2344 (1992).
[18] D. R. Lehman, Phys. Rev. **C25**, 3146 (1982).
[19] D. R. Lehman, M. Rai, and A. Ghovanlou, Phys. Rev. **C17**, 744 (1978).
[20] A. Ghovanlou and D. R. Lehman, Phys. Rev. **C9**, 1730 (1974).
[21] J. Haidenbauer and W. Plessas, Phys.Rev. **C27**, 63 (1983).
[22] J. Haidenbauer, Y. Koike, and W. Plessas, Phys.Rev. **C33**, 439 (1986).
[23] Y. Koike, D. R. Lehman, L. C. Maximon, and W. C. Parke, *Proceedings, 14th International IUPAP Conference on Few Body Problems in Physics (FB14): Williamsburg, Virginia, May 26-31, 1994*, AIP Conf. Proc. **334**, 836 (1995).
[24] Y. Koike, D. R. Lehman, L. C. Maximon, and W. C. Parke, Few Body Syst. **11** (1991).
[25] D. J. Ernst, C. M. Shakin, and R. M. Thaler, Phys.Rev. **C8**, 46 (1973).
[26] L. Hlophe *et al.* (The TORUS Collaboration), Phys.Rev. **C88**, 064608 (2013), arXiv:1310.8334 [nucl-th].
[27] L. Hlophe *et al.* (The TORUS Collaboration), Phys.Rev. **C90**, 061602(R) (2014), arXiv:1409.4012 [nucl-th].
[28] L. Hlophe and C. Elster, Phys. Rev. **C93**, 034601 (2016), arXiv:1512.07084 [nucl-th].
[29] T. Cornelius, W. Gloeckle, J. Haidenbauer, Y. Koike, W. Plessas, and H. Witala, Phys. Rev. **C41**, 2538 (1990).
[30] S. Nemoto, K. Chmielewski, N. W. Schellingerhout, P. U. Sauer, J. Haidenbauer, and S. Oryu, Few Body Syst. **24**, 213 (1998).
[31] H. Kamada, A. Nogga, W. Glöckle, E. Hiyama, M. Kamimura, K. Varga, Y. Suzuki, M. Viviani, A. Kievsky, S. Rosati, J. Carlson, S. C. Pieper, R. B. Wiringa, P. Navrátil, B. R. Barrett, N. Barnea, W. Leidemann, and G. Orlandini, Phys. Rev. C **64**, 044001 (2001).
[32] M. Viviani, A. Deltuva, R. Lazauskas, A. C. Fonseca, A. Kievsky, and L. E. Marcucci, Phys. Rev. C **95**, 034003 (2017).
[33] N. W. Schellingerhout, L. P. Kok, S. A. Coon, and R. M. Adam, Phys. Rev. **C48**, 2714 (1993), [Erratum: Phys. Rev.C52,439(1995)], arXiv:nucl-th/9309012 [nucl-th].
[34] R. Balian and E. Brezin, Nuovo Cim. **B61**, 403 (1969).
[35] E. Schmid and H. Ziegelmann, *The Quantum Mechanical Three-Body Problem*, Vieweg tracts in pure and applied physics (Elsevier, 1974).
[36] Y. Saad, *Iterative Methods for Sparse Linear Systems* (Society for Industrial and Applied Mathematics, SIAM, 2003).
[37] V. I. Kukulin and V. N. Pomerantsev, Annals Phys. **111**, 330 (1978).
[38] I. J. Thompson, B. V. Danilin, V. D. Efros, J. S. Vaagen, J. M. Bang, and M. V. Zhukov, Phys. Rev. **C61**, 024318 (2000).
[39] J. Bang, J. J. Benayoun, C. Gignoux, and I. J. Thompson, Nucl. Phys. **A405**, 126 (1983).
[40] M. Gell-Mann and M. L. Goldberger, Phys. Rev. **91**, 398 (1953).
[41] A. Nogga, R. G. E. Timmermans, and U. van Kolck, Phys. Rev. **C72**, 054006 (2005), arXiv:nucl-th/0506005 [nucl-th].
[42] D. J. Ernst, C. M. Shakin, and R. M. Thaler, Phys.Rev. **C9**, 1780 (1974).
[43] R. Machleidt, Phys. Rev. **C63**, 024001 (2001), arXiv:nucl-th/0006014 [nucl-th].
[44] J. Bang and C. Gignoux, Nucl. Phys. **A313**, 119 (1979).
[45] T. Stammbach and R. Walter, Nuclear Physics A **180**, 225 (1972).
[46] F. Ajzenberg-Selove, Nucl. Phys. **A490**, 1 (1988).
[47] M. V. Zhukov, B. V. Danilin, D. V. Fedorov, J. M. Bang, I. J. Thompson, and J. S. Vaagen, Phys. Rept. **231**, 151 (1993).
[48] V. G. J. Stoks, R. A. M. Klomp, C. P. F. Terheggen, and J. J. de Swart, Phys. Rev. **C49**, 2950 (1994), arXiv:nucl-th/9406039 [nucl-th].
[49] R. B. Wiringa, V. G. J. Stoks, and R. Schiavilla, Phys. Rev. **C51**, 38 (1995), arXiv:nucl-th/9408016 [nucl-th].
[50] D. R. Entem and R. Machleidt, Phys. Rev. **C68**, 041001 (2003), arXiv:nucl-th/0304018 [nucl-th].
[51] W. Glöckle, *The quantum mechanical few-body problem* (Springer, 1983).

label	rank	support energy E_l [MeV]	support momenta k_l [fm^{-1}]
EST3-1	3	$-35, -15, -5$	0.92, 0.60, 0.35
EST3-2	3	$-5, -5, -5,$	0.8, 1.1, 2.5
EST3-3	3	$-25, -5, -5$	0.8, 0.8, 1.1
EST3-4	3	$-65, -10, -10$	0.8, 0.8, 2.5
EST4-1	4	$-20, -3, -3, -3$	0.7, 0.4, 1.1, 2.5
EST4-2	4	$-40, -3, -3, -3$	0.7, 0.4, 1.1, 2.5
EST4-3	4	$-40, -5, -5, -5$	0.7 , 0.4, 1.1, 2.5
EST4-4	4	$-60, -7, -7, -7$	0.7, 0.4, 1.1, 2.5
EST5-1	5	$-30, -20, -3, -3, -3$	0.4, 0.4, 0.4, 1.5, 2.5
EST5-2	5	$-60, -60, -3, -3, -3$	0.5, 0.5, 0.4, 1.5, 2.5
EST5-3	5	$-40, -30, -5, -5, -5$	0.3, 0.3, 0.4, 1.5, 2.5
EST5-4	5	$-60, -40, -5, -5, -5$	0.3, 0.3, 0.4, 1.5, 2.5
EST6-1	6	$-20, -20, -20, -3, -3, -3$	0.4, 1.1, 2.5, 0.4, 1.1, 2.5
EST6-2	6	$-30, -30, -30, -3, -3, -3$	0.4, 1.1, 2.5, 0.4, 1.1, 2.5
EST6-3	6	$-40, -40, -40, -5, -5, -5$	0.4, 1.1, 2.5, 0.4, 1.1, 2.5
EST6-4	6	$-60, -60, -60, -5, -5, -5$	0.4, 1.1, 3.5, 0.4, 1.1, 2.5
EST7-1	7	$-20, -20, -20, -3, -3, -3, -3$	0.4, 1.1, 3.0, 0.4, 1.1, 3.0, 15.0
EST7-2	7	$-30, -30, -30, -3, -3, -3, -3$	0.4, 1.1, 3.0, 0.4, 1.1, 2.5, 15.0
EST7-3	7	$-40, -40, -40, -40, -5, -5, -5$	0.4, 1.1, 3.0, 15.0, 0.4, 1.1, 3.0
EST7-4	7	$-60, -60, -60, -60, -5, -5, -5$	0.4, 1.1, 3.0, 15.0, 0.4, 1.1, 3.0
EST8-1	8	$-60, -60, -60, -60, -5, -5, -5, -5$	0.4, 1.1, 3.0, 15.0, 0.4, 1.1, 3.0, 15.0

TABLE I. Separable representations of the CD-Bonn potential [43] in the energy range $-\infty < E_{2b} \leq -2$ MeV. The labels and ranks of the separable potentials are listed in the first and second column. The corresponding support energies and momenta are given in the third and fourth columns.

label	rank	support energy E_l [MeV]	support momenta k_l [fm^{-1}]
EST3-1	3	$-20, -1, -1$	0.5 0.8, 1.2
EST3-2	3	$-30, -2, -2,$	0.5, 0.8, 1.2
EST3-3	3	$-15, -3, -3$	0.4, 0.4, 2.0
EST3-4	3	$-5, -5, -5$	0.5, 1.2, 2.0
EST4-1	4	$-20, -5, -5, -5$	0.3, 0.8, 1.2, 2.0
EST4-2	4	$-30, -8, -8, -8$	0.4, 0.8, 1.2, 2.0
EST4-3	4	$-40, -12, -12, -12$	0.4, 0.8, 1.2, 2.0
EST4-4	4	$-40, -15, -15, -15$	0.4, 0.8, 1.2, 2.0
EST5-1	5	$-40, -20, -5, -5, -5$	0.3, 0.5, 0.8, 1.2, 2.0
EST5-2	5	$-60, -30, -10, -10, -10$	0.3, 0.5, 0.8, 1.2, 2.0
EST5-3	5	$-40, -40, -3, -3, -3$	0.4, 1.0, 0.8, 1.2, 2.0
EST5-4	5	$-60, -40, -20, -20, -20$	0.4, 0.4, 0.8, 1.2, 2.0
EST6-1	6	$-20, -20, -20, -5, -5, -5$	0.8, 1.1, 2.0, 0.8, 1.2, 2.0
EST6-2	6	$-20, -20, -20, -8, -8, -8$	0.8, 1.1, 2.0, 0.4, 1.1, 2.0
EST6-3	6	$-30, -30, -30, -10, -10, -10$	0.8, 1.1, 3.0, 0.4, 1.1, 2.0
EST6-4	6	$-40, -40, -40, -15, -15, -15$	0.8, 1.1, 3.0, 0.4, 1.1, 2.0
EST7-1	7	$-30, -30, -30, -30, -5, -5, -5$	0.8, 1.1, 2.0, 3.2, 0.4, 1.1, 2.0
EST7-2	7	$-40, -40, -40, -40, -5, -5, -5$	0.8, 1.1, 2.0, 3.2, 0.4, 1.1, 2.0
EST7-3	7	$-50, -50, -50, -50, -10, -10, -10$	0.8, 1.1, 2.0, 3.2, 0.4, 1.1, 2.2
EST7-4	7	$-60, -60, -60, -60, -10, -10, -10$	0.8, 1.1, 2.0, 3.2, 0.4, 1.1, 3.2
EST8-1	8	$-20, -20, -20, -20, -5, -5, -5, -5$	0.8, 1.1, 2.0, 3.2, 0.4, 1.1, 2.0, 3.2
EST8-2	8	$-30, -30, -30, -30, -8, -8, -8, -8$	0.8, 1.1, 2.0, 3.2, 0.4, 1.1, 2.0, 3.2
EST8-3	8	$-50, -50, -50, -50, -10, -10, -10, -10$	0.8, 1.1, 2.0, 3.2, 0.4, 1.1, 2.0, 3.2
EST8-4	8	$-60, -60, -60, -60, -10, -10, -10, -10$	0.8, 1.1, 2.0, 3.2, 0.4, 1.1, 2.0, 3.2

TABLE II. Separable representations of the Bang potential [44] in the energy range $-\infty < E_{2b} \leq -2$ MeV. The labels and ranks of the separable potentials are listed in the first and second column. The corresponding support energies and momenta are given in the third and fourth columns.

label	rank	E_{3b} [MeV]
EST3-1	3	-3.7967
EST3-2	3	-3.7519
EST3-3	3	-3.7507
EST3-4	3	-3.7480
EST4-1	4	-3.7774
EST4-2	4	-3.7737
EST4-3	4	-3.7712
EST4-4	4	-3.7823
EST5-1	5	-3.7847
EST5-2	5	-3.7848
EST5-3	5	-3.7855
EST5-4	5	-3.7845
EST6-1	6	-3.7867
EST6-2	6	-3.7868
EST6-3	6	-3.7871
EST6-4	6	-3.7870
EST7-1	7	-3.7867
EST7-2	7	-3.7867
EST7-3	7	-3.7867
EST7-4	7	-3.7867
EXACT		-3.787

TABLE III. Three-body binding energies for the ground state of ^{6}Li calculated using the separable representations of the CD-Bonn potential listed in Table I. The labels and ranks of the separable potentials are shown in the first and second column. The corresponding three-body binding energies are listed in the third column. The EST8-4 separable representation of the Bang potential defined in Table II is adopted for the $n\alpha$ subsystem. Calculations shown in this table do not include the Coulomb potential.

label	rank	E_{3b} [MeV]
EST3-1	3	-3.7527
EST3-2	3	-3.7524
EST3-3	3	-3.7151
EST3-4	3	-3.7127
EST4-1	4	-3.7788
EST4-2	4	-3.7777
EST4-3	4	-3.7773
EST4-4	4	-3.7778
EST5-1	5	-3.7798
EST5-2	5	-3.7797
EST5-3	5	-3.7807
EST5-4	5	-3.7806
EST6-1	6	-3.7856
EST6-2	6	-3.7852
EST6-3	6	-3.7852
EST6-4	6	-3.7856
EST7-1	7	-3.7868
EST7-2	7	-3.7864
EST7-3	7	-3.7867
EST7-4	7	-3.7865
EST8-1	8	-3.7870
EST8-2	8	-3.7870
EST8-3	8	-3.7866
EST8-4	8	-3.7868
EXACT		-3.787

TABLE IV. Three-body binding energies for the ground state of ^{6}Li calculated using the separable representations of the Bang potential listed in Table II. The labels and ranks of the separable potentials are shown in the first and second columns. The corresponding three-body binding energies are listed in the third column. The EST8-1 separable representation of the CD-Bonn potential defined in Table I is adopted for the *np* subsystem. Calculations shown in this table do not include the Coulomb potential.

λ [fm^{-1}]	$E(\lambda)$ [MeV]	$\langle E(\lambda)\rangle$ [MeV]	$\mathcal{P}_{TDB}(\lambda)$ [%]
0	-35.65	-35.65	89.21
0.01	-32.15	-35.62	88.08
0.1	-4.798	-16.84	30.52
1	-3.842	-3.886	1.133×10^{-2}
10	-3.794	-3.801	1.654×10^{-4}
100	-3.788	-3.789	1.765×10^{-6}
1000	-3.787	-3.788	1.843×10^{-8}
10000	-3.787	-3.787	2.450×10^{-10}
100000	-3.787	-3.787	2.328×10^{-11}
∞	-3.787	-3.787	1.259×10^{-10}

TABLE V. The binding energy of the ground state of ^{6}Li computed with different values of the parameter λ in the projection operator. For this calculation the Coulomb interaction in the $p\alpha$ subsystem is omitted. The quantity $\langle E(\lambda)\rangle$ represents the expectation value of Hamiltonian computed according to Eq. (32) with the corresponding projection. The probability $\mathcal{P}_{TDB}(\lambda)$ defined in Eq. (33) for finding the Pauli forbidden $S_{1/2}$ state in the ^{6}Li ground state wave function is given in the last column.

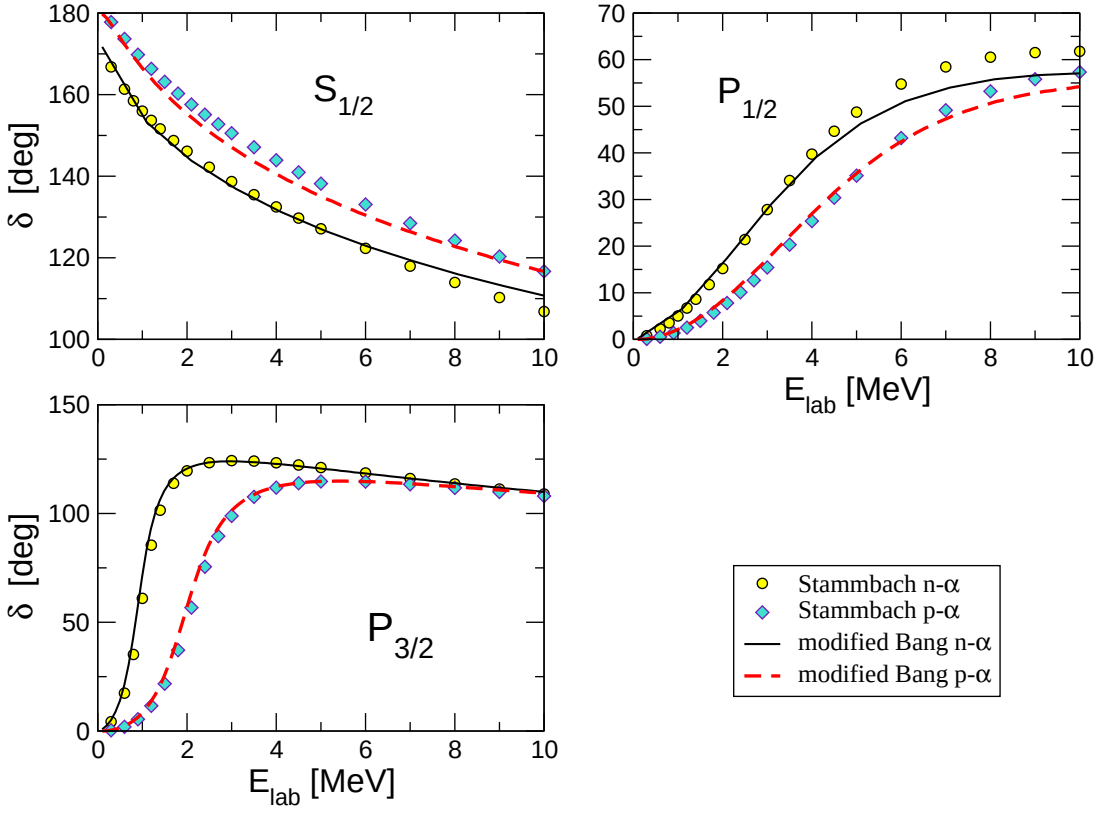

FIG. 1. The S- and P-wave phase shifts in the $n\alpha$ and $p\alpha$ subsystems as function of the neutron/proton laboratory kinetic energy. The solid (dashed) lines represent the calculations with the modified Bang interaction [39] for the $n\alpha$ and $p\alpha$ systems. The phase-shifts extracted from an R-matrix fit [45] are shown for $n\alpha$ by filled circles and for $p\alpha$ by filled diamonds.

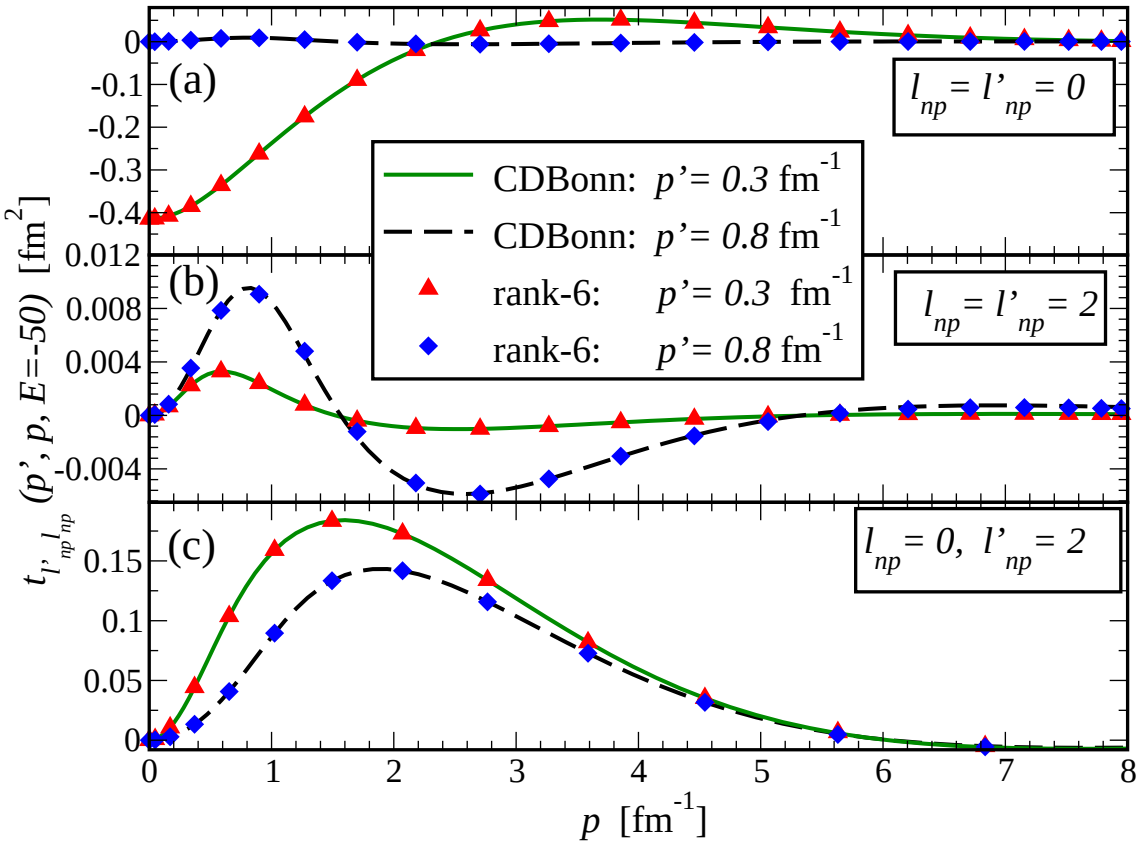

FIG. 2. The off-shell t matrix elements $t_{l'_{np} l_{np}}(p', p; E)$ for the np system as function of the off-shell momentum p. The center of mass energy is E_{2b}= -50 MeV while the total angular momentum and spin are fixed at $J_{np} = S_{np} = 1$. The t matrix elements $t_{00}(p', p; E)$ are shown in panel (a) while the ones corresponding to $l_p = l'_p = 2$ are illustrated in panel (b). Panel (c) shows the matrix elements $t_{20}(p', p; E)$. The solid and dashed lines depict the t matrix elements computed with the CD-Bonn potential for p'= 0.3 fm^{-1} and p'= 0.8 fm^{-1} respectively. The results obtained using a rank-6 separable representation of the CD-Bonn potential are indicated by upward triangles for p'= 0.3 fm^{-1} and by diamonds for p'= 0.8 fm^{-1}. The six EST support points are located at $\{E_l, p_l\} = \{-60, 0.4\}, \{-60, 1.1\}, \{-60, 2.5\}, \{-5, 0.4\}, \{-5, 1.1\}, \{-5, 2.5\}$. The energies have units of MeV while the momenta are given in fm^{-1}.

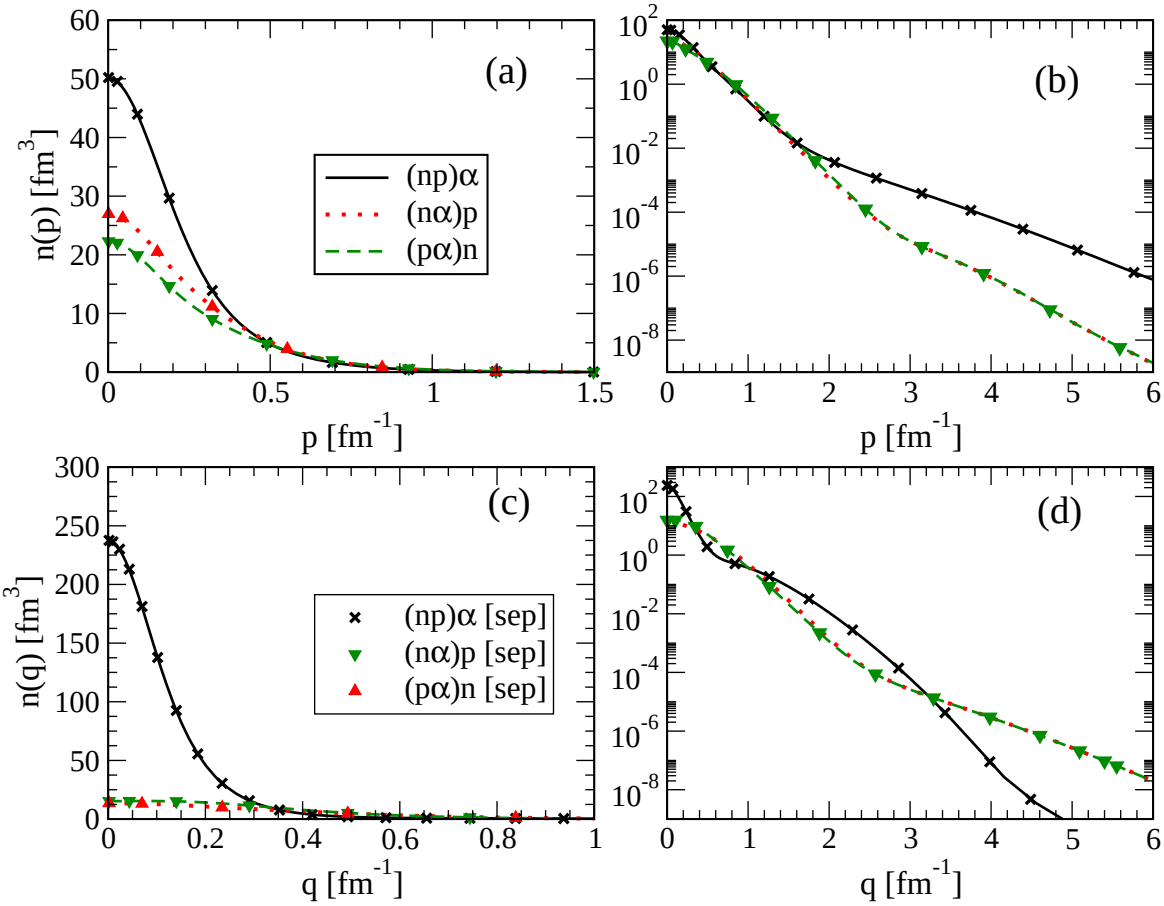

FIG. 3. Panels (a) and (b) show the momentum distributions $n(p)$ in the (np)-α (solid line), $(n\alpha)$-p (dotted line), and $(p\alpha)$-n (dashed line) arrangement channels of the ^{6}Li ground state calculated with the CD-Bonn [43] np interaction and the modified Bang [44] $n\alpha$ interaction. For the $p\alpha$ interaction the Coulomb interaction given in Eq. (29) is added. Panels (c) and (d) show the momentum distributions $n(q)$ for the same arrangement channels as panels (a) and (b). The crosses as well as the upward and downward triangles correspond to the same calculations but using separable forces.

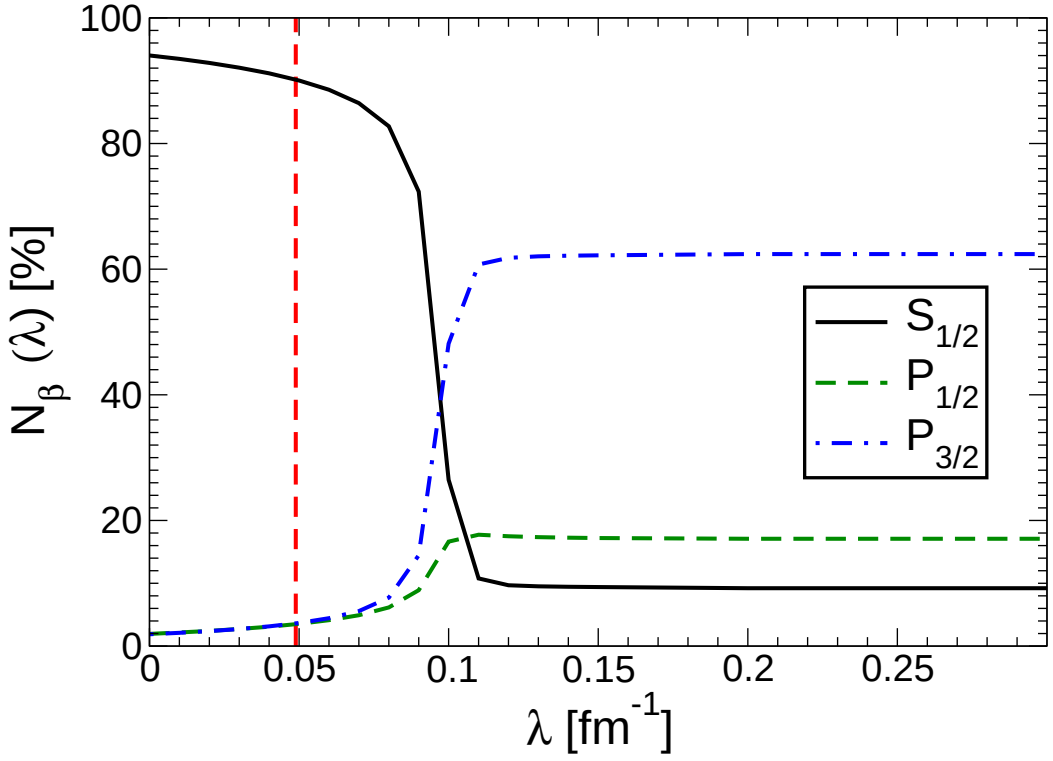

FIG. 4. The probability $N_\beta(\lambda)$ for the ^{6}Li three-body ground state as a function of the projector strength λ calculated according Eq. (34). The solid, dashed, and dot-dashed lines represent the $S_{1/2}$, $P_{1/2}$ and $P_{3/2}$ partial wave states of the $n\alpha$ subsystem. The dashed vertical line indicates the value of λ at which the $S_{1/2}$ state becomes unbound.